Draft version September 19, 2016
Preprint typeset using LaTeX style emulateapj v. 5/2/11

arXiv:1607.01785v2 [astro-ph.GA] 16 Sep 2016

LOW GAS FRACTIONS CONNECT COMPACT STAR-FORMING GALAXIES TO THEIR z ∼ 2 QUIESCENT DESCENDANTS

Justin S. Spilker[1], Rachel Bezanson[1,†], Daniel P. Marrone[1], Benjamin J. Weiner[1], Katherine E. Whitaker[2,†], and Christina C. Williams[1]

Draft version September 19, 2016

ABSTRACT

Early quiescent galaxies at $z \sim 2$ are known to be remarkably compact compared to their nearby counterparts. Possible progenitors of these systems include galaxies that are structurally similar, but are still rapidly forming stars. Here, we present Karl G. Jansky Very Large Array (VLA) observations of the CO(1–0) line towards three such compact, star-forming galaxies at $z \sim 2.3$, significantly detecting one. The VLA observations indicate baryonic gas fractions $\gtrsim$5 times lower and gas depletion times $\gtrsim$10 times shorter than normal, extended massive star-forming galaxies at these redshifts. At their current star formation rates, all three objects will deplete their gas reservoirs within 100 Myr. These objects are among the most gas-poor objects observed at $z > 2$, and are outliers from standard gas scaling relations, a result which remains true regardless of assumptions about the CO-H_2 conversion factor. Our observations are consistent with the idea that compact, star-forming galaxies are in a rapid state of transition to quiescence in tandem with the build-up of the $z \sim 2$ quenched population. In the detected compact galaxy, we see no evidence of rotation or that the CO-emitting gas is spatially extended relative to the stellar light. This casts doubt on recent suggestions that the gas in these compact galaxies is rotating and significantly extended compared to the stars. Instead, we suggest that, at least for this object, the gas is centrally concentrated, and only traces a small fraction of the total galaxy dynamical mass.

Subject headings: galaxies: formation — galaxies: ISM — galaxies: high-redshift

1. INTRODUCTION

Galaxies with large stellar masses ($M_{\rm star} \gtrsim 10^{11}\,M_\odot$) and little ongoing star formation have been observed at redshifts up to $z \sim 4$ (Straatman et al. 2014), and begin to appear in large numbers by $z \sim 2.5$ (e.g., Kriek et al. 2006; Whitaker et al. 2010; Cassata et al. 2013). Many studies have shown that these early quiescent galaxies were much smaller at $z \gtrsim 1.5$ than equally massive star-forming galaxies at similar redshifts (e.g., Trujillo et al. 2007; van der Wel et al. 2014) or quiescent galaxies of similar mass in the local universe (e.g., Daddi et al. 2005; Trujillo et al. 2006; Buitrago et al. 2008; Cimatti et al. 2008; van Dokkum et al. 2008; Damjanov et al. 2011). With effective radii of just $\sim 1-3$ kpc, the stellar densities are of order 100× higher than present-day elliptical galaxies. Similarly massive and compact galaxies are extremely rare in the local universe (e.g., Trujillo et al. 2009; Taylor et al. 2010), implying significant size growth largely consistent with the effects of minor merging (e.g., Trujillo et al. 2011; Newman et al. 2012; see also Carollo et al. 2013). Although not all local massive galaxies had a compact progenitor (e.g., Franx et al. 2008; van Dokkum et al. 2008), most of the $z \sim 2$ compact, massive galaxies likely now reside in the centers of present-day elliptical galaxies (e.g., Bezanson et al. 2009; Belli et al. 2014).

The formation mechanism(s) of the $z \sim 2$ compact quiescent population is still unclear. Recently, however, a population of similarly compact yet highly star-forming galaxies at $z \sim 2.5$ has been identified in deep *Hubble Space Telescope* imaging (Barro et al. 2013, 2014a; Nelson et al. 2014; Williams et al. 2014; van Dokkum et al. 2015). Given their structural similarity, these compact star-forming galaxies (SFGs) are natural candidate progenitors of the early quiescent population, requiring only the cessation of star formation to superficially match the stellar distribution and structure of the $z \sim 2$ quiescent galaxies. Additional evidence from dynamical studies (Barro et al. 2014b; van Dokkum et al. 2015) and number density evolution (Barro et al. 2013) also indicates that compact SFGs will plausibly quench star formation on short timescales ($\lesssim$500 Myr) to build up the growing quiescent population. The small sizes and non-exponential light profiles of compact SFGs present a clear contrast to the typical massive star-forming galaxies at $z \sim 2$, which consist mostly of gas-rich, rapidly rotating disks (e.g., Wuyts et al. 2011; Tacconi et al. 2013; Wisnioski et al. 2015), evidence which suggests very different evolutionary histories.

The aforementioned dynamical studies indicate that the stellar masses of compact SFGs are ubiquitously comparable to or somewhat in excess of simple estimates of the total dynamical masses, $M_{\rm dyn}$, determined through observations of Hα. This implies that the dynamics of compact SFGs are almost completely dominated by the stars – any gas present likely traces, but does not significantly contribute to, the gravitational potential. van Dokkum et al. (2015) argue that the Hα-emitting gas is likely rotating and more extended than the stellar light, preventing the unphysical scenario of $M_{\rm star} > M_{\rm dyn}$. This inference was motivated by observations of veloc-

[1] Steward Observatory, University of Arizona, 933 North Cherry Avenue, Tucson, AZ 85721, USA; jspilker@as.arizona.edu
[2] Department of Astronomy, University of Massachusetts, Amherst, MA 01003, USA
† Hubble Fellow

ity gradients across the slit consistent with rotation for a few objects. Although selection effects are likely in play, these observations imply that the gas is extended by a factor ∼2.5 relative to the stars on average. Adaptive optics-assisted integral-field or interferometric synthesis imaging can be used to spatially and spectrally resolve the gas, providing a more robust tracer of the dynamics than can be inferred from long-slit spectroscopy.

Recent cosmological simulations have matched the observed number counts of compact SFGs and quiescent galaxies (Wellons et al. 2015). This work suggests that the early quiescent population consists mostly of a combination of galaxies which formed their stellar mass early and remained compact since their formation time, and objects which have recently undergone gas-rich major mergers. High-resolution hydrodynamical simulations further indicate that many characteristics of compact massive galaxies can be reproduced through in-situ formation through gas accretion and cooling (e.g., Naab et al. 2009; Feldmann & Mayer 2015), strong central star formation during a gas-rich major merger (e.g., Wuyts et al. 2010; Ceverino et al. 2015), and/or dissipative contraction of gas-rich disks (e.g., Ceverino et al. 2015; Zolotov et al. 2015). In each case, the properties of the gas are key, as its collisional nature allows energy to dissipate and angular momentum to be transferred through the galaxy, permitting the formation of characteristically dense stellar structures.

In this work, we present Karl G. Jansky Very Large Array (VLA) observations of the CO(1–0) line toward three compact SFGs at $z \sim 2.3$. CO(1–0) has long been known as a tracer of molecular hydrogen in the interstellar medium (ISM), the direct fuel from which stars form. If, as we have outlined above, the compact SFGs are in the process of quenching star formation to become $z \sim 2$ quiescent galaxies, we may expect molecular gas properties unlike those of normal SFGs at these redshifts. In particular, if compact SFGs are to quench in tandem with the rapid buildup of the quiescent population, we expect short gas depletion or quenching timescales, indicating that the ongoing high star formation rates (SFRs) cannot be sustained for more than a few hundred Myr.

The outline of this paper is as follows. In Section 2, we describe our sample selection and VLA observations. Section 3 describes our results, including constraints on the molecular gas masses of our targeted objects (Section 3.1), gas fractions and depletion timescales (Section 3.2), and the physical extent of the molecular gas reservoirs in comparison to the stellar light (Section 3.3). We summarize our conclusions in Section 4. Throughout, we assume a flat ΛCDM cosmology, with $H_0 = 67.7\,\mathrm{km\,s^{-1}\ Mpc^{-1}}$ and $\Omega_\mathrm{m} = 0.307$ (Planck Collaboration et al. 2015).

2. DATA

2.1. *Selection of Compact Star-Forming Galaxies*

We selected compact SFGs for VLA CO(1–0) observations from the van Dokkum et al. (2015) sample; detailed selection criteria for the parent sample of compact SFGs are available in that work. In brief, the objects were selected from multi-band photometric catalogs in the CANDELS fields from the 3D-HST program (Koekemoer et al. 2011; Brammer et al. 2012; Skelton et al. 2014; Momcheva et al. 2015) to be massive ($M_\mathrm{star} > 10^{10.6}\,\mathrm{M_\odot}$), compact in WFC3 imaging (van der Wel et al. 2014), and star-forming in rest-frame *UVJ* color-color space. Catalog stellar masses were determined using stellar population synthesis modeling, and SFRs from UV+IR photometry assuming a Chabrier initial mass function, including *Spitzer*/MIPS 24 μm photometry to estimate the dust-obscured SFR of each object (Whitaker et al. 2012, 2014). These SFRs agree well with the 24 μm-based calibrations derived by Rujopakarn et al. (2013). Spectroscopic redshifts of each object were determined through Keck/MOSFIRE or NIRSPEC spectroscopy, detecting Hα and [NII], and are accurate to $\Delta z \sim 0.001$. From the present sample, COSMOS 22995 is identified as an X-ray AGN, while the other two sources are not. We show the selection of compact SFGs in the SFR-M_star (the so-called star-forming main sequence) and $r_\mathrm{eff,F160W}$-M_star planes in Figure 1, highlighting the VLA-observed objects and including later comparison samples.

From this parent sample, we selected northern targets for VLA CO(1–0) observations, preferring objects with high apparent SFRs. The SFR of each target, ranging from $150 - 400\,\mathrm{M_\odot/yr}$ in the 3D-HST catalogs, implied that they likely would not be detected in *Herschel* observations of the GOODS-N and COSMOS fields (Elbaz et al. 2011; Oliver et al. 2012; Roseboom et al. 2012). Indeed, only COSMOS 27289 was detected in any *Herschel*/PACS or SPIRE bands[4]. A simple modified blackbody fit to the FIR photometry indicates $\mathrm{SFR} = 250 \pm 80\,\mathrm{M_\odot/yr}$ for COSMOS 27289, somewhat lower than its SFR in the 3D-HST catalogs. For the other two sources, the *Herschel* non-detections indicate upper limits on the obscured SFR of $\lesssim 200\,\mathrm{M_\odot/yr}$, assuming $T_\mathrm{dust} = 30\,\mathrm{K}$. These upper limits are consistent with the UV+24 μm-derived catalog SFRs. For consistency in our own analysis and with van Dokkum et al. (2015), we use the 3D-HST catalog UV+IR SFRs for all sources.

2.2. *VLA Observations*

VLA observations were carried out between October 2015 and March 2016 under programs 15B-283 and 16A-203 (PI J. Spilker), and are summarized in Table 1. GOODS-N 774 and COSMOS 22995 were observed in the VLA D-configuration (maximum baseline ∼1 km), while COSMOS 27289 was observed in the C-configuration (maximum baseline ∼3.4 km). Complex gain solutions were calculated using the quasars J1148+5924, J1008+062, and J0948+0022 for GOODS-N 774, COSMOS 22995, and COSMOS 27289, respectively, while observations of the quasar 3C286 were used both for bandpass and absolute flux calibration for all sources. The absolute flux scale is estimated to be accurate to 10%. In all cases, the correlator was configured to deliver 2 GHz of continuous bandwidth using the 8-bit samplers, with each baseband pair delivering

[4] Nelson et al. (2014) report detections of GOODS-N 774 in all PACS and SPIRE bands, but we are unable to reproduce their photometry using 24 μm cross-matched *Herschel* catalogs (Roseboom et al. 2012) or by visually inspecting the *Herschel* images. The flux densities reported as significant detections by Nelson et al. (2014) are comparable to or fainter than the quoted *Herschel* map depths. For consistency with the other sources and the 24 μm cross-matched catalogs, we treat this object as undetected by *Herschel*.

Table 1
Summary of VLA Observations

Source	RA	Dec	z^a	Array Configuration	ν_{obs} GHz	Time On-Source h	σ^b μJy beam^{-1}	Beam Size
GOODS-N 774	12h36m27.73s	62°07'12.8"	2.301	D	34.920	1.7	82	2.3×2.6"
COSMOS 22995	10h00m17.15s	2°24'52.3"	2.469	D	33.229	5.1	64	2.6×3.0"
COSMOS 27289	10h00m41.58s	2°27'51.5"	2.234	C	35.644	1.7	92	0.7×0.8"

[a] Spectroscopic redshifts from van Dokkum et al. (2015), determined from Hα and [NII]
[b] rms noise in a 100 km s^{-1} channel

eight dual-polarization basebands of 128 MHz width and 1 MHz channelization. The VLA Ka band receivers were tuned to center the CO(1–0) line in one of these basebands using the Hα-based spectroscopic redshifts of van Dokkum et al. (2015).

After calibration, the data were imaged using natural weighting, which maximizes point-source sensitivity. No source is detected in 9 mm continuum emission, although we serendipitously detected a $S_{35GHz} = 170\,\mu$Jy continuum source in the GOODS-N 774 data located at 12h36m22.50s, +62°06'53.9". This source corresponds to GOODS-N 521 in the 3D-HST catalogs, and appears to be a $z \sim 1.9$ galaxy. No lines are detected in this source, and we will not discuss it further.

Neither GOODS-N 774 or COSMOS 22995 are detected in CO(1–0) emission. For both sources, we extract the spectra shown in Figure 2 by fitting a point source to the visibilities averaged over 24 MHz ($\sim$210 km s^{-1}), fixing the position to the source position in *HST* imaging, using the uncertainty from this procedure to estimate the noise in each channel. The noise is frequency-dependent due to the decline in sensitivity at the edges of each 128 MHz baseband delivered by the VLA correlator. We use these spectra to place upper limits on the integrated CO flux assuming line widths of 500 km s^{-1}, given in Table 2.

COSMOS 27289 is significantly detected in CO(1–0) emission. A naturally-weighted integrated CO image of this galaxy is shown in Figure 3. To determine if COSMOS 27289 is spatially resolved in the C-configuration data, we fit a point source to the visibilities averaged over 100 km s^{-1} centered at the peak of the CO emission. This velocity range encompasses $\sim$95% of the integrated CO emission. No significant residual emission remains. We also examined the visibility amplitudes of the channels with significant line emission as a function of baseline length and found no significant decrease on long baselines, consistent with pointlike source structure. Finally, we created other images of the data applying various tapers in the *uv*-plane. In each case, we recover the same integrated flux density as we measured from the full data. These tests indicate that COSMOS 27289 is not extended at $\sim$0.75" resolution, implying an upper limit on the CO size of $r_{CO} \lesssim 3$ kpc. We extract the spectrum shown in Figure 2 by fitting a point source to the visibilities averaged over 3 MHz ($\sim$25 km s^{-1}), with the position fixed to the peak of the CO emission. We fit a simple Gaussian to this spectrum; the results are listed in Table 2.

3. RESULTS AND DISCUSSION

3.1. *Molecular Gas Masses and the CO-H$_2$ Conversion Factor*

Central to our interpretation of the CO(1–0) observations is the conversion factor from CO luminosity to molecular gas mass, α_{CO}. The CO-H$_2$ conversion factor is known to vary with the metallicity and kinematic state of the molecular gas (for a recent review, see Bolatto et al. 2013). For star-forming galaxies near solar metallicity, the value of α_{CO} ranges from $\sim$0.8 M$_\odot$ (K km s^{-1} pc^2)$^{-1}$ in highly star-forming objects (e.g., Downes & Solomon 1998) to $\sim$4 M$_\odot$ (K km s^{-1} pc^2)$^{-1}$ in the Milky Way and nearby quiescently star-forming galaxies (e.g., Sandstrom et al. 2013; hereafter we suppress the units of α_{CO}).

The appropriate value of α_{CO} in compact SFGs is not immediately obvious, but we can estimate its value and plausible upper and lower bounds through several methods. First, both the mass-metallicity relation and the [NII]/Hα line ratios of our sources indicate that the metallicity of each source is approximately solar or slightly super-solar (Pettini & Pagel 2004; Mannucci et al. 2010). In this regime, variations in α_{CO} are no longer significantly affected by metallicity; instead, variations are driven by optical depth and/or excitation effects. This implies that α_{CO} is almost certainly not significantly higher than the galactic value, $\alpha_{CO} \sim 4$. Several authors have derived theoretical or empirical formulations of the dependence of α_{CO} on metallicity (e.g., Wolfire et al. 2010; Glover & Mac Low 2011; Feldmann et al. 2012) which also indicate that $\alpha_{CO} \sim 4$ is a reasonable upper limit for galaxies of approximately solar metallicity.

We can place further limits on α_{CO} by following the discussion of Narayanan et al. (2012b). These authors derived a fitting formula for α_{CO} using hydrodynamical simulations of isolated and merging systems coupled with line and dust radiative transfer. This fitting formula depends on both the galaxy metallicity and the CO surface brightness, where objects with higher CO surface brightness have lower conversion factors. For the two non-detections, we assume that the extent of the CO(1–0) emission is at least as large as the stellar emission seen in *HST*, which is nearly always observed (e.g., Tacconi et al. 2013; Spilker et al. 2015). This places an upper limit on the CO surface brightness. At solar metallicity, our two non-detections imply conversion factors $\alpha_{CO} \gtrsim 0.7$. For COSMOS 27289, in contrast, our data place an upper limit on α_{CO}. In this case, because the CO(1–0) emission is unresolved at 0.75" resolution, the Narayanan et al. (2012b) fitting formula implies $\alpha_{CO} \lesssim 1.6$.

Finally, we can derive an empirical estimate of α_{CO} by noting that it appears to correlate well with galaxy SFR or L_{IR} (Spilker et al. 2015), based on a compilation of estimates of α_{CO} in $z > 1$ objects using vari-

Table 2
Observational Results

Source	$M_{\rm star}$ $10^{11}\,{\rm M}_\odot$	$r_{\rm eff,F160W}$ kpc	SFR ${\rm M}_\odot$/yr	$L'_{\rm CO(1-0)}$ $10^{10}\,{\rm K\,km\,s^{-1}\ pc^2}$	FWHM$_{\rm CO}$ ${\rm km\,s^{-1}}$
GOODS-N 774	1.0	1.0	150	< 1.4	
COSMOS 22995	1.2	1.1	190	< 1.3	
COSMOS 27289	1.3	2.3	400	1.3 ± 0.3	60±18

Note. — Stellar masses are from the 3D-HST catalogs (Brammer et al. 2012; Skelton et al. 2014), source sizes from van der Wel et al. (2014), and SFRs from Whitaker et al. (2014). We list 3σ $L'_{\rm CO(1-0)}$ upper limits for the two non-detections, assuming a line width of $500\,{\rm km\,s^{-1}}$, approximately the median Hα FWHM of the van Dokkum et al. (2015) sample. These $L'_{\rm CO(1-0)}$ values are equivalent to $M_{\rm gas}$ under the assumption of $\alpha_{\rm CO} = 1\,{\rm M}_\odot\ ({\rm K\,km\,s^{-1}\ pc^2})^{-1}$; see Section 3.1.

ous techniques from the literature, including dust-based, dynamics-based, and CO surface brightness-based methods. For the objects in our sample, this correlation implies $\alpha_{\rm CO} \sim 1-3$, in reasonable agreement with our previous estimates.

In summary, all indications are that the CO-H_2 conversion factor is expected to be relatively low in these highly star-forming objects. For simplicity we adopt $\alpha_{\rm CO} = 1$ for the remainder of this work. For COSMOS 27289, this results in $M_{\rm gas} = (1.3 \pm 0.3) \times 10^{10}\,{\rm M}_\odot$, and 3σ upper limits of $M_{\rm gas} < 1.3 \times 10^{10}$ and $< 1.4 \times 10^{10}\,{\rm M}_\odot$ for COSMOS 22995 and GOODS-N 774, respectively, integrating over a $500\,{\rm km\,s^{-1}}$ line width (approximately the median Hα FWHM of the van Dokkum et al. 2015 sample). We reiterate that these measurements carry significant systematic uncertainties, likely at least a factor of two. Future observations may help clarify the interpretation of CO(1–0) in compact SFGs by spatially and spectrally resolving the objects (yielding a dynamical constraint on $\alpha_{\rm CO}$) or using observations of the long-wavelength dust continuum and dust-to-gas ratio arguments to derive alternate estimates of $M_{\rm gas}$.

3.2. *Molecular Gas Fractions and Depletion Timescales*

Using the molecular gas masses derived in the previous section, in Figure 4 we compare the baryonic gas fractions $f_{\rm gas} \equiv M_{\rm gas}/(M_{\rm star} + M_{\rm gas})$ of the compact SFGs with those derived for both $z \sim 1-3$ normal, main-sequence galaxies (Daddi et al. 2010; Tacconi et al. 2013) and $z \sim 1-4$ dusty, star-forming galaxies (DSFGs; compiled from Swinbank et al. 2010; Ivison et al. 2011, 2013; Fu et al. 2012, 2013; Magnelli et al. 2012; Magdis et al. 2012; Hodge et al. 2013; Ma et al. 2015; Aravena et al. 2016). Gas masses for all objects were derived from CO (although largely from higher-excitation transitions instead of the ground state in the main-sequence sample), and all measurements are subject to significant systematic uncertainties. From this figure it is clear that the compact SFGs in our sample are severe outliers from other $z \sim 2$ populations, even though the compact SFGs generally lie near the star-forming main sequence (Figure 1; see also Whitaker et al. 2012; Barro et al. 2014b). With gas fractions $\lesssim$12%, the compact SFGs are among the most gas-poor objects observed at $z \sim 2$, in stark contrast to the high gas fractions ubiquitously observed at these redshifts (though see also Narayanan et al. 2012a). Even if we adopt a Milky Way-like $\alpha_{\rm CO} = 4$, the inferred baryonic gas fractions are $\lesssim$30%, lower than 90% of the CO-observed comparison sample objects. In other words, the compact SFGs we have observed are genuinely deficient in CO emission, regardless of its conversion to $M_{\rm gas}$.

A consequence of their low gas masses accompanied by rapid star formation is that the compact SFGs we have observed are similar outliers from main sequence populations in the Schmidt-Kennicutt relation between SFR and $M_{\rm gas}$ and in their gas depletion timescales, $t_{\rm dep} \equiv M_{\rm gas}/{\rm SFR}$, as shown in Figure 5. In this respect, the compact SFGs appear analogous to the highly star-forming DSFGs, with depletion times $\lesssim 10^8$ yr. Whether the similar depletion times between compact SFGs and DSFGs is due to similar star-forming conditions in these objects is unclear. The low gas masses of compact SFGs indicate that they can undergo little further mass growth without replenishment of their gas reservoirs, in contrast to DSFGs, which have typical high gas fractions (Figure 4). The low gas fractions of compact SFGs seem to indicate that they are elevated relative to most objects on the Schmidt relation not because they exhibit very efficient star formation (high SFR at a given $M_{\rm gas}$), but because they are about to exhaust their gas reservoirs (low $M_{\rm gas}$ at a given SFR).

Some authors have suggested an evolutionary connection between DSFGs and the $z \sim 2$ compact quiescent population (e.g., Blain et al. 2004; Tacconi et al. 2008; Toft et al. 2014) based in part on the observed small sizes of DSFGs (e.g., Simpson et al. 2015; Spilker et al. 2016). The low gas masses of compact SFGs indicate that they may be transitioning below the main sequence, perhaps shortly after the end of the submillimeter-luminous phase. Only ∼15% of compact SFGs are detected in *Herschel*/SPIRE images (Barro et al. 2014a), consistent with this interpretation. Unfortunately, we have essentially no constraint on the past star formation in these objects, making it difficult to know if the compact SFGs were once DSFGs.

In both gas fraction and depletion time, the compact SFGs are outliers by factors of ∼5 to >10 from standard gas scaling relations (e.g., Genzel et al. 2015), indicating that these relations are not applicable to this unusual population of galaxies. This result holds even if we adopt a galactic $\alpha_{\rm CO} = 4$, in which case compact SFGs still have gas fractions ∼2× lower and depletion times ∼3× lower than massive $z \sim 2.3$ main sequence galaxies. Taken together, Figures 4 and 5 indicate that the compact SFGs we have selected are indeed consistent with

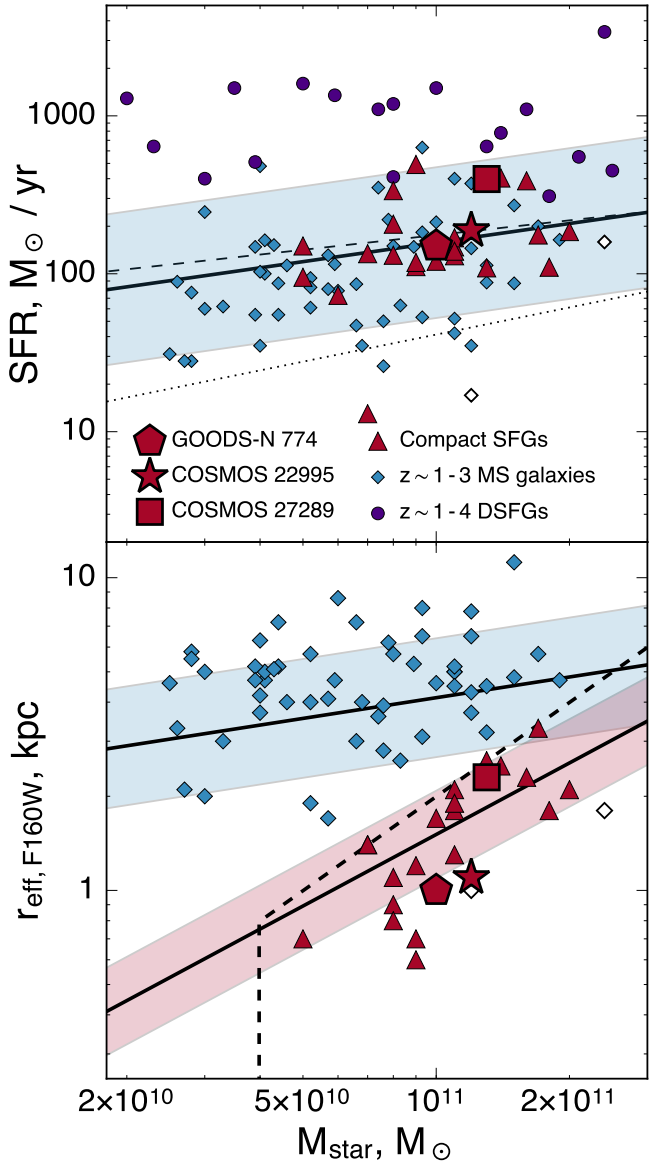

Figure 1. Selection of compact SFGs. In both panels, the full sample of van Dokkum et al. (2015) is shown as red triangles, while the objects observed by the VLA are shown with larger symbols and individually labeled. Comparison samples of CO-observed $z \sim 1-3$ main sequence (MS) galaxies and $z \sim 1-4$ dusty, star-forming galaxies (DSFGs) are shown as blue diamonds and navy circles, respectively; these samples are described further in Section 3.2. Within the main sequence sample, two objects would also be selected as compact SFGs; these objects are shown with open symbols here and in Figures 4 and 5. *Top:* The compact SFGs lie generally near the star-forming main sequence. The dotted, solid, and dashed black lines show the main sequence at redshifts 1, 2.3, and 3, respectively, as derived by Whitaker et al. (2012), while the blue shaded region denotes SFRs a factor of 3 above and below the $z = 2.3$ relation. Note that the SFR of massive main sequence galaxies increases by approximately a factor of 4 over the redshift range spanned by the main-sequence comparison sample, $z \sim 1-3$. *Bottom:* The compact SFGs have similar structural properties as quiescent galaxies at these redshifts. The blue and red regions show the size–mass relations derived for star-forming and quiescent galaxies at $z \sim 2.25$, respectively, by van der Wel et al. (2014). The size–mass selection criterion used by van Dokkum et al. (2015) is marked with a dashed black line.

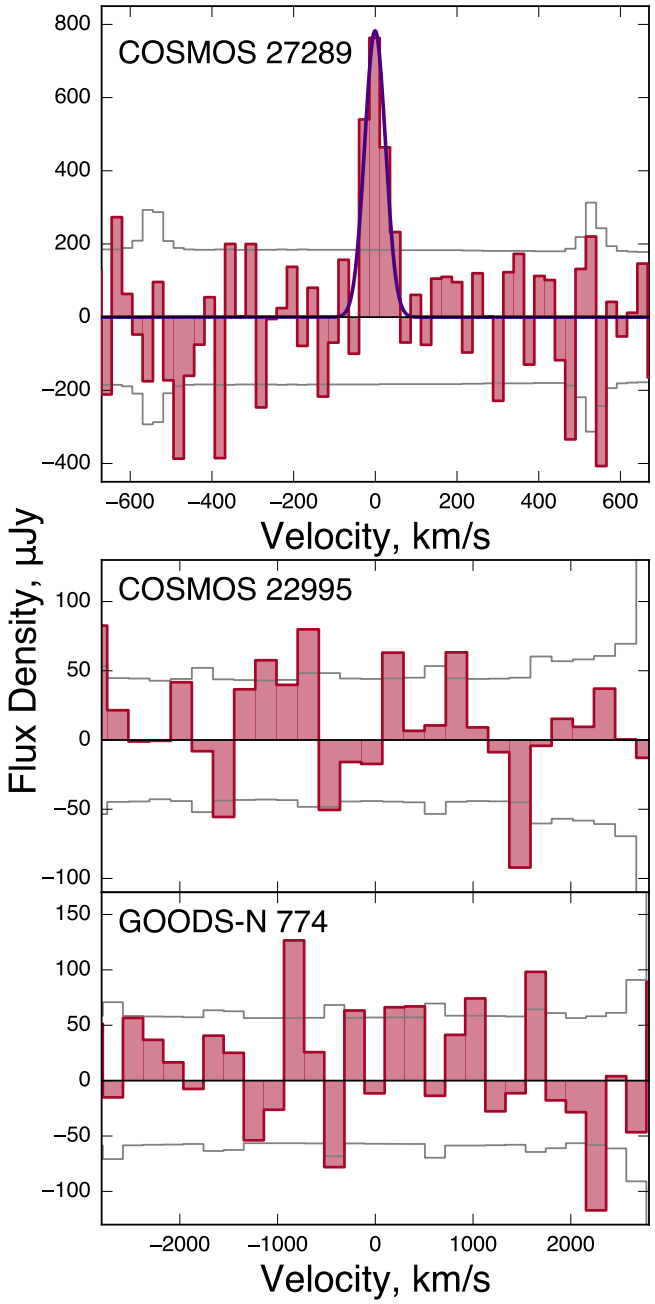

Figure 2. CO(1–0) spectra of the three sources observed in this work, derived by fitting a point source to the visibilities of each channel. For each source, we show the spectrum in red, with the frequency-dependent $\pm 1\sigma$ noise as thin gray lines. For COSMOS 27289, the spectrum is shown at 3 MHz ($\sim$25 km s^{-1}) resolution, and the best-fit Gaussian profile is shown in navy. For the other two sources, the spectra are plotted in 24 MHz ($\sim$210 km s^{-1}) channels.

being the immediate progenitors of some fraction of the $z \sim 2$ quiescent population, in a state of rapid transition. If the current SFR continues at its present rate with no further gas accretion, each object we have observed will deplete its gas supply before $z = 2$, presumably dropping below the star-forming main sequence at the same time. Our depletion time estimates could be lengthened if the SFR is declining and continues to decline as the gas supply is exhausted, but it is clear that compact SFGs can add very little additional stellar mass through star formation without substantial gas accretion.

The low measured gas fractions and short depletion times are consistent with the inferences made by Barro

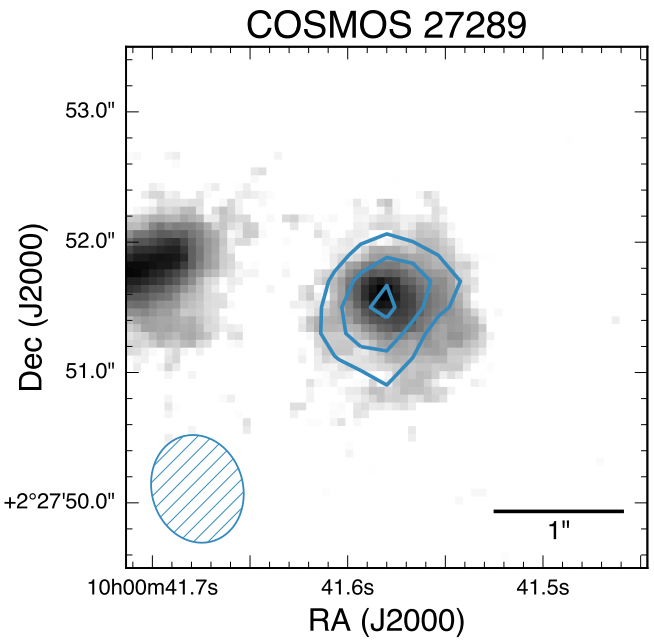

Figure 3. Contours of the CO(1–0) emission in COSMOS 27289 are overlaid on the *HST*/F160W image of this object. The CO emission is averaged over 12 MHz ($\sim$100 km s^{-1}) centered on the line peak, and contours are drawn at 3, 5, and 7σ. The synthesized beam in this naturally-weighted image is shown in the lower left.

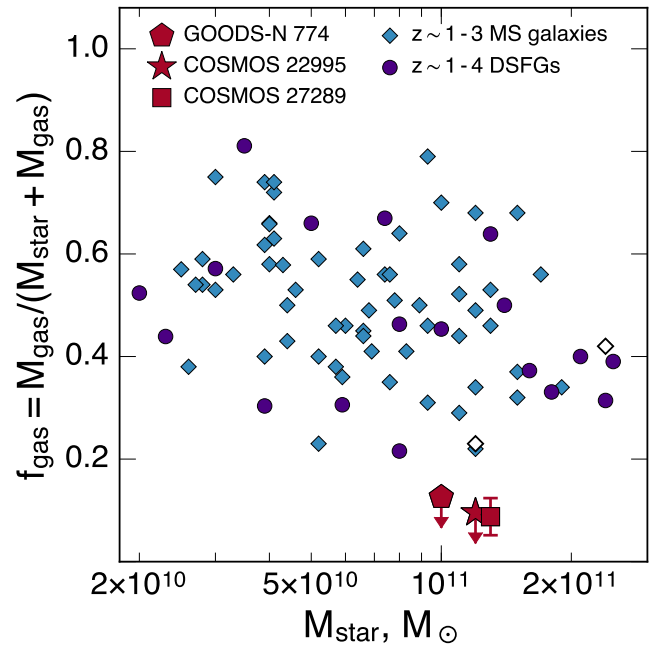

Figure 4. The gas fractions $f_{\rm gas}$ observed for the compact SFGs observed in this work (red symbols, assuming $\alpha_{\rm CO} = 1$; see Section 3.1), compared to those measured for $z \sim 1-3$ main-sequence (light blue diamonds) and starbursting galaxies (dark blue circles). The non-detections are 3σ upper limits. The compact SFGs we have observed have very low gas fractions compared to any other objects at these redshifts with measured gas masses, a result which holds even if we adopt a Milky Way-like $\alpha_{\rm CO}$. Open symbols are the two main sequence comparison objects which also meet the compactness selection criterion (Figure 1).

et al. (2014b), who noted that simple dynamical mass estimates are frequently close to or lower than the stellar masses inferred from population synthesis models, implying gas fractions $f_{\rm gas} \lesssim$30%. A similar conclusion was inferred by van Dokkum et al. (2015), who estimated gas fractions $f_{\rm gas} \lesssim$40%. Our results indicate even smaller gas fractions than estimated by these authors, affirming the conclusion that these galaxies have likely nearly exhausted their gas reservoirs and are either currently quenching or about to quench. The details of this quenching process are testable using higher spatial resolution observations. Observations of the dust continuum and high-resolution CO imaging would indicate whether the currently ongoing SFR and the reservoir of remaining gas are concentrated in the galaxy outskirts or the central regions. Such observations would provide a relatively straightforward test of theoretical models, which generally predict inside-out quenching (e.g., Zolotov et al. 2015).

3.3. *A Compact Gas Reservoir in COSMOS 27289*

We significantly detected CO(1–0) emission in COSMOS 27289, finding a line width FWHM of 60 $\pm$ 18 km s^{-1}. The Hα line observed by van Dokkum et al. (2015) was somewhat broader, 130 $\pm$ 30 km s^{-1} (though note this line was only marginally spectrally resolved; the NIRSPEC instrumental resolution at this wavelength is $\sim$ 80 km s^{-1}). If real, the difference in line width between CO(1–0) and Hα may indicate that the CO-emitting gas is slightly more compact than the Hα-emitting gas, or that the Hα line is somewhat contaminated by nuclear emission. Our C array observations did not spatially resolve the source in CO. This implies an upper limit on the CO-emitting region of $r_{\rm CO} \lesssim$ 3 kpc. Our ability to distinguish velocity gradients is somewhat hampered by low signal-to-noise, but we similarly see no strong evidence for a gradient that would be consistent with a rotating disk or any other organized velocity structure. Across the line profile, the emission centroid changes position by $\lesssim$0.8" ($\lesssim$7 kpc). In other words, our data offer no evidence that the CO-emitting gas is extended relative to the stellar emission ($r_{\rm eff,F160W}$ = 2.3 kpc), and only weak evidence of different spatial distributions of the CO- and Hα-emitting gas.

At least in this single case, our result contrasts with conclusion of van Dokkum et al. (2015), who inferred that compact SFGs host rotating gas disks which are more extended than the stellar distributions by an average factor of $\sim$2.3. This inference was motivated by noting that compact SFG gas velocity dispersions are systematically lower than expected from their stellar masses and sizes (equivalently, that stellar masses are higher than simple dynamical mass estimates), and supported by the observation that some objects showed Hα velocity gradients across the slit consistent with rotation. For COSMOS 27289, the gas radius that reconciles the stellar and dynamical masses is $\sim$20 kpc (van Dokkum et al. 2015). At this large radius, the rotation curve implied by the stellar mass has fallen to match the low velocity measurement, but at the price of assuming that dark matter is negligible within 20 kpc. However, such a large gas radius would have been easily detectable in our data. For this object, invoking a large, rotating gas disk is not supported by the data.

How, then, can the discrepant dynamical and stellar mass estimates be reconciled? A simple, but unsat-

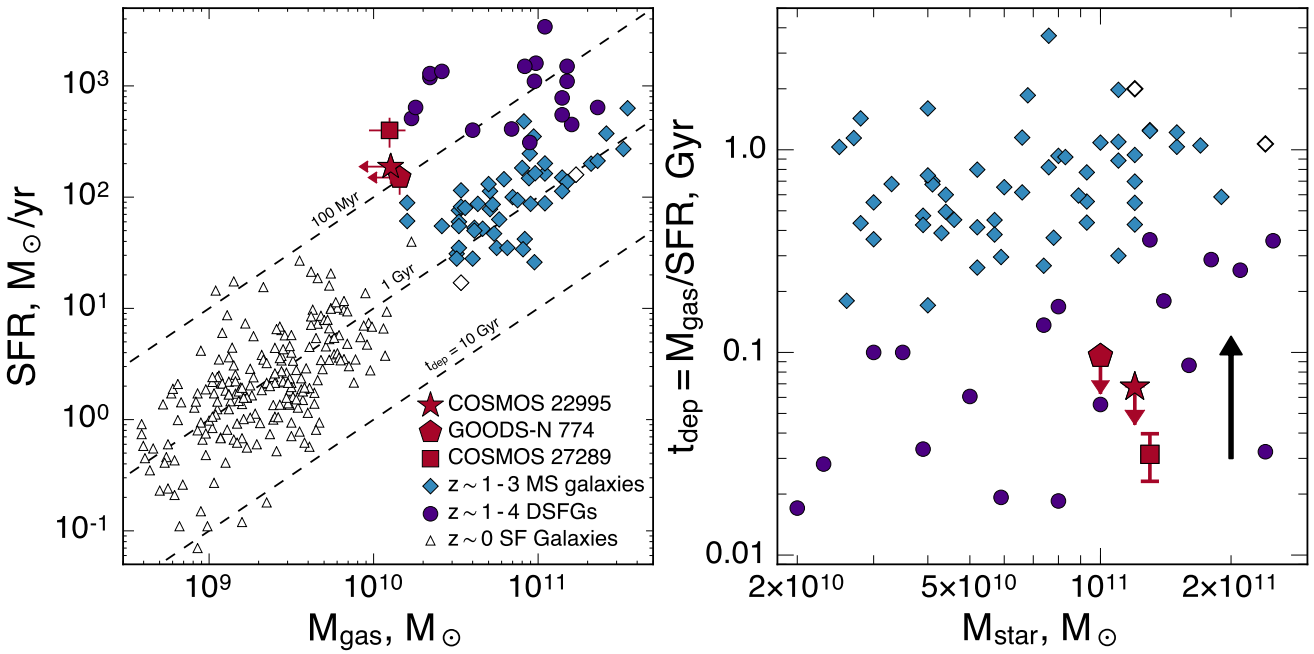

Figure 5. *Left:* The integrated Schmidt-Kennicutt relation between SFR and $M_{\rm gas}$, with symbols as in Figure 4. We additionally include the $z \sim 0$ sample of star-forming galaxies of Saintonge et al. 2011 (white triangles), and show lines of constant $t_{\rm dep}$ (dashed). *Right:* The gas depletion times $t_{\rm dep}$ as a function of $M_{\rm star}$, assuming the star formation in each object continues at its present rate. The compact SFGs we have observed show depletion times much shorter than typical galaxies at these redshifts, consistent with a rapid transition to quiescence. The arrow indicates the effect of adopting a galactic CO–H_2 conversion factor $\alpha_{\rm CO} = 4$.

isfying explanation is that COSMOS 27289 is an outlier in terms of kinematic geometry or stellar mass estimate. $M_{\rm dyn}$ depends on the assumed galaxy geometry and dynamics, resulting in factor of 2 systematic uncertainties. COSMOS 27289 may be an outlier compared to the assumed-disk-like overall population, or it may be that compact SFGs are not well-described by simple disk- or dispersion-dominated geometries (if, for example, they are generally recent merger remnants; Wellons et al. 2015). If COSMOS 27289 does have disk-like dynamics, it may be face-on, although its axis ratio in the rest-frame optical implies an inclination of $\sim$45° (van Dokkum et al. 2015). Second, we cannot rule out the possibility that stellar masses have been systematically overestimated in compact SFGs (but are accurate for most normal galaxies). If this is the case, the tension with the dynamical masses would be lowered while also bringing the gas fractions nearer to the value expected for normal, extended star-forming galaxies at this epoch. Given the extensive photometry and grism spectroscopy available for the extragalactic legacy fields in which compact SFGs have been selected, however, this seems unlikely.

A more likely solution is that the CO-emitting gas does not trace the full galaxy dynamical (or stellar) mass. The calculations of van Dokkum et al. (2015) required a very extended gas disk because of their assumption that the gas velocity dispersion must trace the full stellar mass of the compact SFGs – for a given dynamical model, if the total mass and circular velocity are fixed, the only remaining free parameter is the galaxy radius. Instead, our data paint a different picture. Given that the observed gas radius and velocity dispersion are small, the gas likely only traces a small fraction of the total galaxy mass in the central regions. In other words, instead of fixing the total mass and velocity dispersion to infer large radii, we argue that the mass interior to the gas effective radius is much lower than the full stellar mass, removing the need to invoke large gas disks to reconcile the stellar and dynamical masses.

In addition to our own data, this scenario is supported by the recent observations of Barro et al. (2016), who observed that the stellar absorption lines were nearly 70% broader than the gas nebular emission lines in a compact SFG at $z = 1.7$. This difference increases the dynamical mass inferred from the stars by nearly a factor of 3, and prevents the unphysical scenario of $M_{\rm star} > M_{\rm dyn}$. A similar effect is likely at work in COSMOS 27289, predicting that future ultra-deep NIR spectroscopy will find a stellar velocity dispersion in excess of the gas velocity dispersion. More immediate progress may be made by continued CO observations using either higher-resolution B array observations or simply deeper observations with the current C array.

Having only detected and placed constraints on the dynamics of a single object, we cannot draw strong conclusions concerning the discrepancy between stellar and dynamical masses in the compact SFG population as a whole. While larger samples of objects with spatially and spectrally resolved spectroscopy will be required to investigate this issue further, it is clear that even relatively modest upper limits on the spatial extent of the molecular gas provide powerful constraints on the gas dynamics of compact SFGs.

4. CONCLUSIONS

We have observed the CO(1–0) transition in three $z \sim 2.3$ compact star-forming galaxies in an effort to determine the amount of molecular gas in these objects. Our two non-detections and one detected source confirm low baryonic gas fractions and very short gas depletion timescales, as expected if compact SFGs are currently

or on the verge of quenching star formation. The gas fractions and depletion times are much lower than predicted from gas scaling relations. In the detected galaxy, we see no evidence that the CO-emitting gas is spatially extended relative to the stellar light, and only weak evidence for a difference in the CO dynamics compared to the Hα emission. This result demonstrates that invoking large gas disks to increase dynamical masses estimated from gas kinematics above the stellar masses may not be warranted. Instead, we argue that the gas is centrally concentrated, and therefore need not kinematically trace the full stellar mass of compact SFGs. An increased sample size and high-resolution follow-up observations of the molecular gas content of compact SFGs would indicate whether this is true of the bulk of the population or if COSMOS 27289 is an outlier.

J.S.S. and D.P.M. acknowledge support from the U.S. National Science Foundation under grant No. AST-1312950. R.B. and K.E.W. gratefully acknowledge support by NASA through Hubble Fellowship grants #HF-51318 and #HF-51368 awarded by the Space Telescope Science Institute, which is operated by the Association of Universities for Research in Astronomy, Inc., for NASA, under contract NAS5-26555. C.C.W. was supported by the NIRCam contract to the University of Arizona, NAS5-02015. The National Radio Astronomy Observatory is a facility of the National Science Foundation operated under cooperative agreement by Associated Universities, Inc. This work is based on observations taken by the 3D-HST Treasury Program (GO 12177 and 12328) with the NASA/ESA HST, which is operated by the Association of Universities for Research in Astronomy, Inc., under NASA contract NAS5-26555. This research has made use of NASA's Astrophysics Data System.

Facility: VLA

REFERENCES

Aravena, M., Spilker, J. S., Bethermin, M., et al. 2016, MNRAS, 457, 4406
Barro, G., Faber, S. M., Pérez-González, P. G., et al. 2013, ApJ, 765, 104
—. 2014a, ApJ, 791, 52
Barro, G., Trump, J. R., Koo, D. C., et al. 2014b, ApJ, 795, 145
Barro, G., Faber, S. M., Dekel, A., et al. 2016, ApJ, 820, 120
Belli, S., Newman, A. B., & Ellis, R. S. 2014, ApJ, 783, 117
Bezanson, R., van Dokkum, P. G., Tal, T., et al. 2009, ApJ, 697, 1290
Blain, A. W., Chapman, S. C., Smail, I., & Ivison, R. 2004, ApJ, 611, 725
Bolatto, A. D., Wolfire, M., & Leroy, A. K. 2013, ARA&A, 51, 207
Brammer, G. B., van Dokkum, P. G., Franx, M., et al. 2012, ApJS, 200, 13
Buitrago, F., Trujillo, I., Conselice, C. J., et al. 2008, ApJ, 687, L61
Carollo, C. M., Bschorr, T. J., Renzini, A., et al. 2013, ApJ, 773, 112
Cassata, P., Giavalisco, M., Williams, C. C., et al. 2013, ApJ, 775, 106
Ceverino, D., Sanchez-Almeida, J., Muñoz-Tuñon, C., et al. 2015, ArXiv e-prints, arXiv:1509.02051
Cimatti, A., Cassata, P., Pozzetti, L., et al. 2008, A&A, 482, 21
Daddi, E., Renzini, A., Pirzkal, N., et al. 2005, ApJ, 626, 680
Daddi, E., Bournaud, F., Walter, F., et al. 2010, ApJ, 713, 686
Damjanov, I., Abraham, R. G., Glazebrook, K., et al. 2011, ApJ, 739, L44
Downes, D., & Solomon, P. M. 1998, ApJ, 507, 615
Elbaz, D., Dickinson, M., Hwang, H. S., et al. 2011, A&A, 533, A119
Feldmann, R., Gnedin, N. Y., & Kravtsov, A. V. 2012, ApJ, 747, 124
Feldmann, R., & Mayer, L. 2015, MNRAS, 446, 1939
Franx, M., van Dokkum, P. G., Förster Schreiber, N. M., et al. 2008, ApJ, 688, 770
Fu, H., Jullo, E., Cooray, A., et al. 2012, ApJ, 753, 134
Fu, H., Cooray, A., Feruglio, C., et al. 2013, Nature, 498, 338
Genzel, R., Tacconi, L. J., Lutz, D., et al. 2015, ApJ, 800, 20
Glover, S. C. O., & Mac Low, M.-M. 2011, MNRAS, 412, 337
Hodge, J. A., Carilli, C. L., Walter, F., Daddi, E., & Riechers, D. 2013, ApJ, 776, 22
Ivison, R. J., Papadopoulos, P. P., Smail, I., et al. 2011, MNRAS, 412, 1913
Ivison, R. J., Swinbank, A. M., Smail, I., et al. 2013, ApJ, 772, 137
Koekemoer, A. M., Faber, S. M., Ferguson, H. C., et al. 2011, ApJS, 197, 36
Kriek, M., van Dokkum, P. G., Franx, M., et al. 2006, ApJ, 649, L71
Ma, J., Gonzalez, A. H., Spilker, J. S., et al. 2015, ApJ, 812, 88
Magdis, G. E., Daddi, E., Béthermin, M., et al. 2012, ApJ, 760, 6
Magnelli, B., Saintonge, A., Lutz, D., et al. 2012, A&A, 548, A22
Mannucci, F., Cresci, G., Maiolino, R., Marconi, A., & Gnerucci, A. 2010, MNRAS, 408, 2115
Momcheva, I. G., Brammer, G. B., van Dokkum, P. G., et al. 2015, ArXiv e-prints, arXiv:1510.02106
Naab, T., Johansson, P. H., & Ostriker, J. P. 2009, ApJ, 699, L178
Narayanan, D., Bothwell, M., & Davé, R. 2012a, MNRAS, 426, 1178
Narayanan, D., Krumholz, M. R., Ostriker, E. C., & Hernquist, L. 2012b, MNRAS, 421, 3127
Nelson, E., van Dokkum, P., Franx, M., et al. 2014, Nature, 513, 394
Newman, A. B., Ellis, R. S., Bundy, K., & Treu, T. 2012, ApJ, 746, 162
Oliver, S. J., Bock, J., Altieri, B., et al. 2012, MNRAS, 424, 1614
Pettini, M., & Pagel, B. E. J. 2004, MNRAS, 348, L59
Planck Collaboration, Ade, P. A. R., Aghanim, N., et al. 2015, ArXiv e-prints, arXiv:1502.01589
Roseboom, I. G., Ivison, R. J., Greve, T. R., et al. 2012, MNRAS, 419, 2758
Rujopakarn, W., Rieke, G. H., Weiner, B. J., et al. 2013, ApJ, 767, 73
Saintonge, A., Kauffmann, G., Kramer, C., et al. 2011, MNRAS, 415, 32
Sandstrom, K. M., Leroy, A. K., Walter, F., et al. 2013, ApJ, 777, 5
Simpson, J. M., Smail, I., Swinbank, A. M., et al. 2015, ApJ, 807, 128
Skelton, R. E., Whitaker, K. E., Momcheva, I. G., et al. 2014, ApJS, 214, 24
Spilker, J. S., Aravena, M., Marrone, D. P., et al. 2015, ApJ, 811, 124
Spilker, J. S., Marrone, D. P., Aravena, M., et al. 2016, ApJ, 826, 112
Straatman, C. M. S., Labbé, I., Spitler, L. R., et al. 2014, ApJ, 783, L14
Swinbank, A. M., Smail, I., Longmore, S., et al. 2010, Nature, 464, 733
Tacconi, L. J., Genzel, R., Smail, I., et al. 2008, ApJ, 680, 246
Tacconi, L. J., Neri, R., Genzel, R., et al. 2013, ApJ, 768, 74
Taylor, E. N., Franx, M., Glazebrook, K., et al. 2010, ApJ, 720, 723
Toft, S., Smolčić, V., Magnelli, B., et al. 2014, ApJ, 782, 68
Trujillo, I., Cenarro, A. J., de Lorenzo-Cáceres, A., et al. 2009, ApJ, 692, L118
Trujillo, I., Conselice, C. J., Bundy, K., et al. 2007, MNRAS, 382, 109
Trujillo, I., Ferreras, I., & de La Rosa, I. G. 2011, MNRAS, 415, 3903
Trujillo, I., Feulner, G., Goranova, Y., et al. 2006, MNRAS, 373, L36

van der Wel, A., Franx, M., van Dokkum, P. G., et al. 2014, ApJ, 788, 28
van Dokkum, P. G., Franx, M., Kriek, M., et al. 2008, ApJ, 677, L5
van Dokkum, P. G., Nelson, E. J., Franx, M., et al. 2015, ApJ, 813, 23
Wellons, S., Torrey, P., Ma, C.-P., et al. 2015, MNRAS, 449, 361
Whitaker, K. E., van Dokkum, P. G., Brammer, G., & Franx, M. 2012, ApJ, 754, L29
Whitaker, K. E., van Dokkum, P. G., Brammer, G., et al. 2010, ApJ, 719, 1715
Whitaker, K. E., Franx, M., Leja, J., et al. 2014, ApJ, 795, 104
Williams, C. C., Giavalisco, M., Cassata, P., et al. 2014, ApJ, 780, 1
Wisnioski, E., Förster Schreiber, N. M., Wuyts, S., et al. 2015, ApJ, 799, 209
Wolfire, M. G., Hollenbach, D., & McKee, C. F. 2010, ApJ, 716, 1191
Wuyts, S., Cox, T. J., Hayward, C. C., et al. 2010, ApJ, 722, 1666
Wuyts, S., Förster Schreiber, N. M., van der Wel, A., et al. 2011, ApJ, 742, 96
Zolotov, A., Dekel, A., Mandelker, N., et al. 2015, MNRAS, 450, 2327